Smart Structures and Systems, *Vol. 15, No. 4 (2015) 1103-1120*
DOI: http://dx.doi.org/10.12989/sss.2015.15.4.1103

Characterization and modeling of a self-sensing MR damper under harmonic loading

Z.H. Chen[1a], Y.Q. Ni[*2] and S.W. Or[3b]

[1]*College of Civil Engineering, Fuzhou University, Fuzhou, 350116 Fujian, China*
[2]*Department of Civil and Environmental Engineering, The Hong Kong Polytechnic University, Hung Hom, Kowloon, Hong Kong*
[3]*Department of Electrical Engineering, The Hong Kong Polytechnic University, Hung Hom, Kowloon, Hong Kong*

(Received May 19, 2014, Revised October 19, 2014, Accepted November 10, 2014)

Abstract. A self-sensing magnetorheological (MR) damper with embedded piezoelectric force sensor has recently been devised to facilitate real-time close-looped control of structural vibration in a simple and reliable manner. The development and characterization of the self-sensing MR damper are presented based on experimental work, which demonstrates its reliable force sensing and controllable damping capabilities. With the use of experimental data acquired under harmonic loading, a nonparametric dynamic model is formulated to portray the nonlinear behaviors of the self-sensing MR damper based on NARX modeling and neural network techniques. The Bayesian regularization is adopted in the network training procedure to eschew overfitting problem and enhance generalization. Verification results indicate that the developed NARX network model accurately describes the forward dynamics of the self-sensing MR damper and has superior prediction performance and generalization capability over a Bouc-Wen parametric model.

Keywords: self-sensing magnetorheological (MR) damper; piezoelectric force sensor; dynamic modeling; hysteresis; NARX neural network; Bayesian regularization

1. Introduction

Semi-active control systems that offer the reliability of passive control systems as well as the versatility and adaptability of active control systems have received significant attention for structural vibration control worldwide (Jung *et al.* 2004). Magnetorheological (MR) fluid dampers have emerged as such a class of semi-active damping devices. By activating the MR fluid contained in the device through its magnetic field, it can reversibly change from liquid to semisolid in milliseconds, which results in a continuously controllable device with considerable bandwidth. MR dampers require minute power for field activation and are insensitive to impurity penetration commonly encountered during manufacture and usage (Carlson *et al.* 1996). More importantly, they are inherently fail-safe devices in that they can still operate as passive dampers

*Corresponding author, Professor, E-mail: ceyqni@polyu.edu.hk
[a] Assistant Professor, E-mail: zhchen.ethan@gmail.com
[b] Professor, E-mail: eeswor@polyu.edu.hk

http://www.techno-press.org/?journal=sss&subpage=8 ISSN: 1738-1584 (Print), 1738-1991 (Online)

once the control hardware fails (Dyke *et al.* 1996, Spencer *et al.* 1997). Recognizing the attractive characteristics and promising potential of the MR-based damping technique, global researchers and engineers have investigated the feasibility and application of MR dampers in a wide variety of areas, such as seismic protection of building and bridge structures (Dyke *et al.* 1996, Gordaninejad *et al.* 2002, Fujitani *et al.* 2003, Jung *et al.* 2003, Ni *et al.* 2004, Ying *et al.* 2005, Loh *et al.* 2007), vibration control of bridge cables (Johnson *et al.* 2000, Ko *et al.* 2002, Duan *et al.* 2005, Weber *et al.* 2005b, Li *et al.* 2007), vibration damping of suspension systems of trains and vehicles (Liao and Wang 2003, Song *et al.* 2005, Choi *et al.* 2009) and stability augmentation of helicopters (Gandhi *et al.* 2001, Hu and Wereley 2008).

In spite of the abovementioned advantages, existing MR dampers are incapable of monitoring structural vibration, external loadings or their damping forces, and hence require extra sensors for realizing closed-loop feedback control. As a consequence, they are used as adjustable passive dampers in an open-loop mode in a certain current practices of civil structural control, like in vibration mitigation of bridge cables (Chen *et al.* 2004, Weber *et al.* 2005a), which hinders full utilization of their controllable damping capability. To advance the MR damper based structural control from an open-loop operation to a closed-loop manner, a novel self-sensing MR damper possessed of a sensing-while-damping functionality has been devised with a piezoelectric force sensor embedded inside the device (Or *et al.* 2008).

MR dampers demonstrate highly nonlinear behaviors because of the inherent non-Newtonian nature of MR fluid. Hence, it is challenging to formulate models that accurately represent their nonlinear dynamics. Such models are essential in understanding the operation principles of the devices and in developing robust control strategies that take full advantage of their unique features. Various parametric models, which are described by an arrangement of mechanical elements such as masses, springs and dashpots, have been developed (Spencer *et al.* 1997, Pang *et al.* 1998, Jiménez and Álvarez-Icaza 2005, Ikhouane and Dyke 2007, Boston *et al.* 2010). The parametric model structures are typically determined by a trial-and-error iterative procedure and with some heuristics, based on the qualitative interpretation of measurement data. In order to account for the complex phenomena such as nonlinear and hysteretic behaviors, additional nonlinear blocks, such as Bingham model, Bouc-Wen model, Dahl friction model and LuGre friction model, have been included frequently. Optimizing the parameters of the highly nonlinear model structures, therefore, requires sophisticated identification methods, in which intelligently selected initial points or proper constraints on the parameters are usually necessary to avoid divergence or local minima.

Alternative representations of MR damper dynamics using nonparametric methods have been proposed to eliminate some pitfalls of the parametric approaches in terms of artificial neural network (Chang and Roschke 1998, Wang and Liao 2005, Cao *et al.* 2008, Boada *et al.* 2010), neuro-fuzzy inference system (Schurter and Roschke 2000, Ahn *et al.* 2009), polynomial NARX (nonlinear autoregressive with exogenous inputs) modeling (Leva and Piroddi 2002), and wavelet-based identification (Jin *et al.* 2005, Karimi *et al.* 2009), etc. The majority of the previous studies in the context of nonparametric modeling have been made by using numerical simulation data rather than using real experimental data of MR dampers. In addition, neural networks are commonly believed to prone to overfitting, which results in overparameterized models that fail to generalize to novel situations. The previous works rarely addressed on overfitting or generalization issue in training neural networks to identify the dynamics of MR dampers, which may give rise to questionable stability or reliability problem in the control application associated with the overfitted models.

This paper presents the development and characterization of a self-sensing MR damper, and

then addresses the modeling of its forward dynamics by means of an NARX-based neural network technique. NARX model is employed due to both its capability of capturing a wide variety of nonlinear dynamic behaviors and the availability of identification algorithms in a reasonable computational cost (Chen *et al.* 1990). A multilayer perceptron (MLP), a class of feed-forward artificial neural networks, is then used to identify the NARX model in that it is a universal approximator for any continuous nonlinear function (Hornik *et al.* 1989). The synthesized technique, named NARX network, results in a powerful model structure that is able to represent complex nonlinear behaviors, such as chaos, hysteresis, saturation effects and combinations of several nonlinear phenomena (Suykens *et al.* 1996). To derive a robust model with low complexity and good generalization capability, the topology of the NARX network is optimized and the Bayesian regularization technique (MacKay 1992) is incorporated in the NARX network learning process to eschew overfitting. Comparison of the prediction performance is also made between the NARX network model and a Bouc-Wen based parametric model.

2. Characterization of self-sensing MR damper

2.1 Self-sensing MR damper

Fig. 1 displays a prototype of a self-sensing MR damper, which is fabricated by integrating a piezoelectric force sensor with a conventional actuation-only MR damper. The damper comprises an electromagnet, a diaphragm, an accumulator, a bearing and seal unit, a piston and MR fluid, which are housed in a metallic main cylinder, as well as a pair of electrical wires extended from the electromagnet and through the piston. It is 208 mm in total length and has a ±25 mm stroke. The magnetic field strength inside the device can be varied by supplying input currents through the electrical wires with the maximum of 1 A and 2 A for continuous and intermittent working situations, respectively.

Fig. 2 shows the detailed configuration of the embedded piezoelectric force sensor. Components of the sensor include a lead zirconate titanate (PZT) piezoceramic wafer, two electrode wafers, two insulating wafers, two metal adaptors, a pair of signal wires and a threaded bolt. These components are sandwiched centrally in a stack between the adaptors by using the bolt. Good surface finishing on the neighboring faces of the two adaptors is made to ensure high reliability and sensitivity of the piezoelectric sensor. Since the piezoelectric sensor works properly only under compression, the technique of mechanical prestressing is performed on the sensor so that tension forces can be measured while the piezoelectric element remains in compression during operation. The prestressing is carried out by employing a torque driver to produce a compression stress of 18 MPa on the piezoelectric wafer with a calibrated torque of 30 N·m. The torque is slowly exerted by the torque driver to the bolt until it is overloaded. During this procedure, the positive and negative electrodes are connected to form a short-circuit condition to avoid accumulation of charges on the surfaces of the piezoelectric wafer. The assembled sensor is then calibrated (as detailed in the next section) before it is embedded with the damper part to form the prototype as shown in Fig. 1.

In operation, the embedded force sensor senses the variation of force imposed on the damper during structural vibration. The sensed signals are then used to assist in adjusting the current input to the damper through an appropriate control strategy and thereby the commanded damping force. The self-sensing MR damper thus has the dual function of force sensing while controllable

damping.

2.2 Calibration of piezoelectric force sensor

The fabricated piezoelectric force sensor is calibrated by evaluating its charge-to-force sensitivity prior to its integration with the damper part. The calibration test is conducted on a servohydraulic material testing system (MTS) operated in force-controlled mode. The charges produced by the piezoelectric sensor due to the external excitation forces are measured through a charge meter. The output charge and input force signals are sampled at 1 kHz and recorded by a data acquisition system.

In calibration, the MTS machine is commanded to generate sinusoidal force excitations exerted on the sensor structure with frequencies of 0.2, 1.0, 2.5 and 5.0 Hz and amplitudes of 500, 1000, 1500 and 2000 N. Experimental data are used to investigate the relationship between the MTS driving force and the output charge produced from the piezoelectric sensor. The acquired data are filtered using an elliptic lowpass filter to remove any undesirable noises above 20 Hz. Fig. 3 shows the time domain signals of the driving force and the output charge for a selected calibration case under a sinusoidal force excitation with frequency of 2.5 Hz and amplitude of 1000 N. For other calibration cases, similar results are obtained as plotted in Fig. 3. It is observed that for each case there is always a phase difference of 90° between the charge and the force. The relationship between charge and force is linear for each calibration case with a nearly identical slope.

Based on the linear relationship between the charge (Q_{PZT}) and the force (F_{MTS}), the sensitivity of the piezoelectric force sensor, defined by the charge-to-force factor (k_{PZT}), can be derived as

Fig. 1 Prototype of self-sensing MR damper

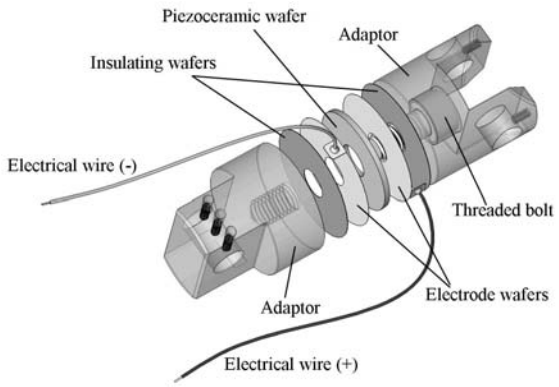

Fig. 2 Assembly diagram of piezoelectric force sensor

$$k_{\mathrm{PZT}} = \frac{\sum_{i=1}^{n} Q_{\mathrm{PZT}}\big|_i^2}{\sum_{i=1}^{n} (Q_{\mathrm{PZT}}\big|_i \cdot F_{\mathrm{MTS}}\big|_i)} \tag{1}$$

where n is the total number of data samples used for the calibration. To quantify the accuracy of the sensitivity, a normalized root mean square (RMS) deviation is defined as

$$\delta_1 = \frac{\sqrt{\frac{1}{n}\sum_{i=1}^{n}\left(F_{\mathrm{PZT}}\big|_i - \frac{Q_{\mathrm{PZT}}\big|_i}{k_{\mathrm{PZT}}}\right)^2}}{\sqrt{\frac{1}{n}\sum_{i=1}^{n}(F_{\mathrm{MTS}}\big|_i - \overline{F}_{\mathrm{MTS}})^2}} \tag{2}$$

where $\overline{F}_{\mathrm{MTS}}$ is the mean value of the input force.

The calibrated sensitivity k_{PZT} and the corresponding normalized RMS deviation δ_1 are calculated for all calibration cases (with different combinations of frequency from 0.2 Hz to 5.0 Hz and excitation amplitude from 500 N to 2000 N). It is found that the variation of the sensitivity for all test cases is reasonably small with the values of δ_1 less than 4%. Consequently, the sensitivity coefficient for the piezoelectric force sensor is averaged from all the calibration results to be $\overline{k}_{\mathrm{PZT}} = -158.248$ pC/N with a normalized RMS deviation of 2.35%. In application, as long as the piezoelectric charge output from the piezoelectric force sensor is sensed, the external force can be measured with the following correlation

$$F_{\mathrm{PZT}} = \frac{Q_{\mathrm{PZT}}}{\overline{k}_{\mathrm{PZT}}} \tag{3}$$

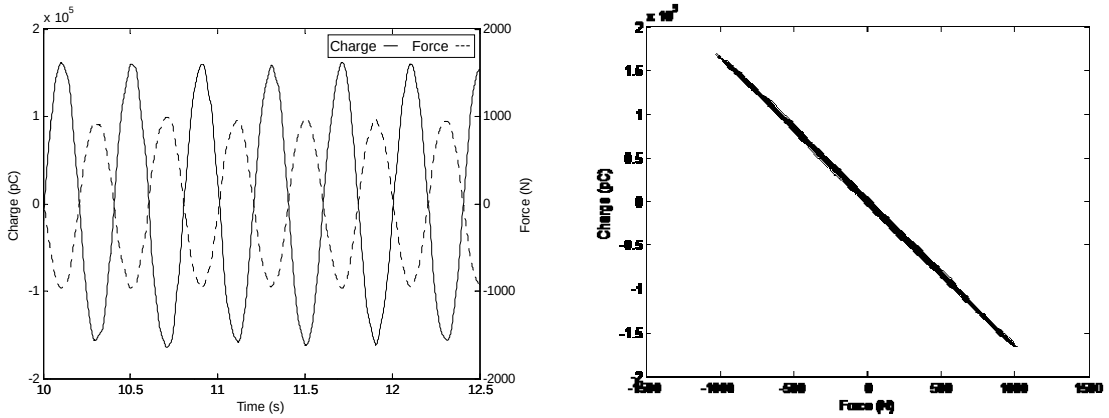

(a) Charge and force in time domain (b) Charge-force relationship

Fig. 3 Calibration of piezoelectric force sensor under force-controlled sinusoidal excitation with frequency of 2.5 Hz and amplitude of 1000 N

2.3 Performance of self-sensing MR damper

To evaluate the force sensing capability and damping behaviors of the self-sensing MR damper, performance tests are carried out on the whole device by operating the MTS machine in displacement-controlled mode. The displacement excitation is manipulated in sinusoidal waveform with different frequencies and amplitudes, and the current input to the damper is set at different constant levels via a direct current (DC) power supplier. The damper force sensed by the piezoelectric force sensor, the displacement excitation and the reaction force measured with the transducer embedded in the MTS are recorded by the data acquisition system for analysis.

The sensing performance of the device is assessed by the degree of agreement between the force signals from the piezoelectric force sensor and the MTS load cell, which is defined by another normalized RMS deviation of

$$\delta_2 = \frac{\sqrt{\frac{1}{m}\sum_{j=1}^{m}(F_{\mathrm{MTS}}|_j - F_{\mathrm{PZT}}|_j)^2}}{\sqrt{\frac{1}{m}\sum_{j=1}^{m}F_{\mathrm{MTS}}|_j^2}} \tag{4}$$

in which m is the total number of data samples used in the calculation.

Fig. 4 shows the experimental results obtained from the performance tests, in which a sinusoidal displacement-controlled excitation with frequency of 5.0 Hz and amplitude of 5.0 mm is exerted on the damper powered with DC current levels of 0, 0.5 and 1.0 A, respectively. A good agreement is observed between the force signals of F_{PZT} and F_{MTS}, and is also evidenced in Table 1 with small values of the normalized RMS deviation δ_2. The measured results therefore verify the reliable force sensing capability of the devised self-sensing MR damper.

The controllable damping behaviors of the self-sensing MR damper are examined in terms of the measured force-displacement and force-velocity trajectories. Fig. 5 displays the hysteresis behaviors of the MR damper subjected to a sinusoidal displacement-controlled excitation with frequency of 5.0 Hz and amplitude of 5.0 mm and different input currents from 0 A to 1.0 A. It is observed that the damper force has a dependency on the applied current level for activating the magnetic field to energize the MR fluid. In the absence of the field strength at 0 A, the damper force mainly results from the viscous behavior of the MR fluid together with the friction between the damper rod and the bearing and seal unit. The magnitude of the damper force then increases with the increment of the applied current, but the increase slows down when the current approaches to 1.0 A due to the gradual magnetic saturation effect of the MR fluid. In addition, the areas enclosed by the force-displacement and force-velocity hysteresis loops enlarge with the increasing current, indicating the enhanced capability of vibrational energy dissipation provided by the damper. Therefore, the damping performance provided by the self-sensing MR damper is controllable through adjusting the current strength, but it is also limited by the residual state and the magnetic saturation of the damper.

Table 1 Normalized RMS deviations in performance tests

Current (A)	0	0.25	0.5	0.75	1.0
δ_2 (%)	3.89	2.70	2.30	2.46	2.39

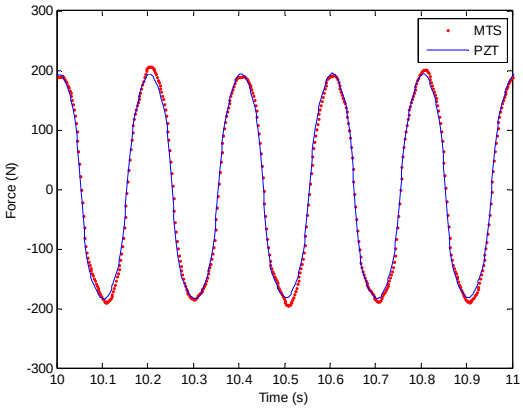

(a) 0.0 A

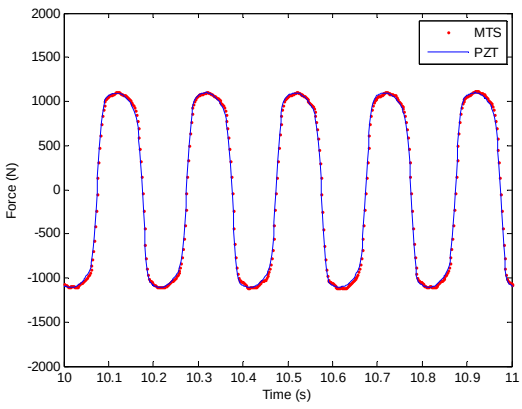

(b) 0.5 A

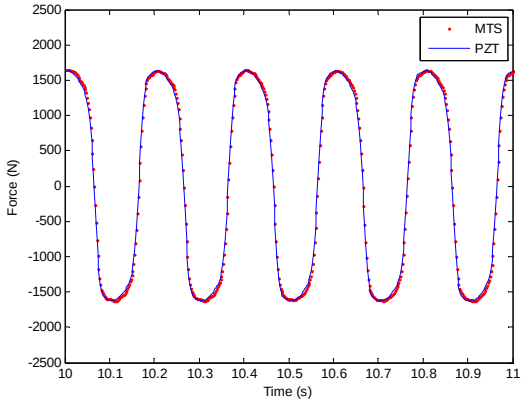

(c) 1.0 A

Fig. 4 Validation of force sensing capability under 5.0 Hz, 5.0 mm sinusoidal displacement excitation with different current levels

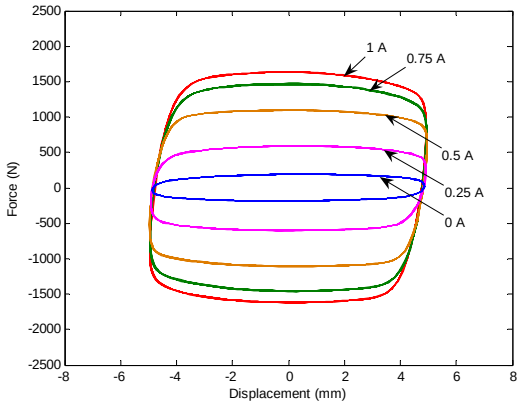

(a) Force versus displacement

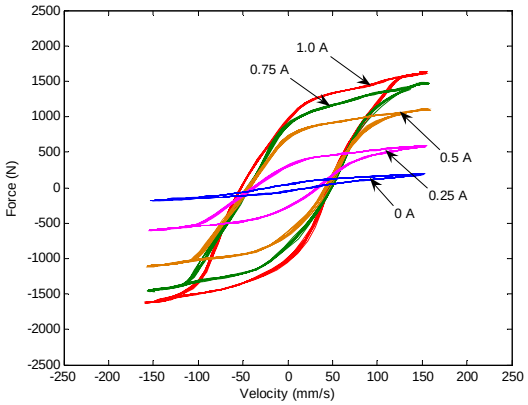

(b) Force versus velocity

Fig. 5 Hysteresis behaviors of self-sensing MR damper

3. Modeling of self-sensing MR damper

3.1 Model formulation

As observed in Fig. 5, the self-sensing MR damper is a highly nonlinear device and hence the modeling of its dynamic behaviors is a non-trivial task. In this study, an NARX network model which integrates the NARX modeling and neural network techniques is developed to emulate the self-sensing MR damper. The proposed model is formulated as

$$\hat{F}(t) = f(x(t), \cdots, x(t-n_x), \dot{x}(t), \cdots, \dot{x}(t-n_{\dot{x}}), F(t-1), \cdots, F(t-1-n_F); \boldsymbol{\theta}) \tag{5}$$

where x, $\dot{x}$ and F are the displacement and velocity of the damper piston and the sensed damper force, respectively; n_x, $n_{\dot{x}}$ and n_F denote lag spaces of the displacement, velocity and damper force, respectively; and $f(\cdot;\boldsymbol{\theta})$ represents a nonlinear parametric function in terms of the displacement and velocity at present and previous time steps and the damping force at previous time steps, and is identified by an MLP; and $\boldsymbol{\theta}$ is a parameter vector including weights and biases of the MLP. The parameters can be derived by training the NARX network to minimize a typical objective function, namely, the sum of squared error between the target and the network prediction

$$E_D = \sum_{t=1}^{T} [F(t) - \hat{F}(t)]^2 \tag{6}$$

3.2 Parameter identification

Due to its fast convergence property, the Levenberg-Marquardt algorithm (Hagan and Menhaj 1994) has been widely used for network training to identify and update the network parameters. During training, the objective function (6) is minimized. The nonlinear properties of neural network allow fitting the training set to very small errors. However, overfitting problem occurs when the training error is minimized to an extreme value; thus the generated model fails to generalize to unseen data well. One approach to ameliorating network generalization capability, referred to as regularization (Sjöberg and Ljung 1995), is to constrain the growth of network parameters by expanding the objective function (6) as

$$E_R = \beta E_D + \alpha E_\theta \tag{7}$$

where $E_\theta = \sum_{i=1}^{M} \theta_i^2$ is the sum of square of the network parameters, M is the total number of the parameters, β and α are regularization parameters which control the flexibility of the model and are objectives of the network optimization process.

Within the Bayesian framework, MacKay (1992) interpreted network learning as an inference of the most plausible network parameters given the training data and optimized the regularization parameters by finding their most probable values, which are derived as

$$\alpha^{\mathrm{MP}} = \frac{\gamma}{2E_\theta}, \quad \beta^{\mathrm{MP}} = \frac{N-\gamma}{2E_D} \tag{8a, b}$$

where $\gamma = M - 2\alpha \cdot \text{trace}(\mathbf{H}^{-1})$ measures the effective number of network parameters involved in reducing the objective function, and **H** is the Hessian matrix of the objective function (7). In training implementation, with an initial guess of α and β, the Levenberg-Marquardt algorithm is employed to find the most plausible network parameters to minimize the objective function defined in Eq. (7). The use of the Levenberg-Marquardt algorithm can also overcome the costly computation of the Hessian matrix and its inverse by making a Gauss-Newton approximation to the Hessian matrix (Foresee and Hagan 1997). During the training process, re-estimation of α and β is executed automatically to obtain their most plausible values according to the implicit formulae given in Eq. (8). It is suggested that all data sets be scaled into the range of [-1, 1] to avoid that some network parameters will be trained to be extremely large or small to accommodate different scales of input and target variables. In addition, the procedure of multiple random initializations of network parameters is used to retrain the network to assure that the optimal solution, instead of local minimum, has been reached during the training phase.

3.3 Network architecture

According to Eq. (5), a three-layer NARX network with S_1 ($= n_x + n_{\dot{x}} + n_F + 3$) neurons in the input layer, S_2 neurons in the hidden layer and one neuron in the output layer, is employed to map the input-output relationship of the self-sensing MR damper. The input variables in the model will be selected from the displacement x and velocity $\dot{x}$ of the damper piston at present and previous time steps and the sensed damper force F at previous time steps to predict the one-step-ahead damper force. Transfer functions in the hidden and output layers are selected as a hyperbolic tangent sigmoid function and a linear function, respectively, with the forms of

$$g_1(u_1) = \frac{1 - \exp(-2u_1)}{1 + \exp(-2u_1)}, \quad g_2(u_2) = u_2 \tag{9a, b}$$

Experimental data collected from the displacement-controlled tests performed on the self-sensing MR damper are used as training, validation and testing data sets for the NARX network modeling. The model is first trained using the training data through the Bayesian regularized learning procedure, with its architecture being determined using the validation data. The well-trained model is then exposed to the testing data unseen during the training phase to examine its generalization capability. In the case of constant input current I = 0.5 A, recorded signals under sinusoidal excitations with frequency of 1.0 Hz, amplitude of 1.0 mm and with frequency of 5.0 Hz, amplitude of 5.0 mm are taken as the training data, while the validation data set includes signals collected under sinusoidal excitations with frequency of 1.0 Hz, amplitude of 5.0 mm and with frequency of 5.0 Hz, amplitude of 1.0 mm.

To assess the prediction performance of the resulting NARX network model, the root mean square error (RMSE) between the measured damper force and the prediction from the model is evaluated by

$$\text{RMSE} = \sqrt{\frac{1}{T}\sum_{t=1}^{T}[F(t) - \hat{F}(t)]^2} \tag{10}$$

An appropriate architecture of the NARX network is important to realize good modeling performance. To optimize input variables for the NARX network, the sensitivity of the model with

respect to different input configurations of displacement (x), velocity ($\dot{x}$) and past value of damper force (F) is examined. The resulting model performance evaluated on the validation data set is compared in Fig. 6. It is apparent that the model performance is poor if only the displacement x and velocity $\dot{x}$ are used as the network input. Hence, incorporation of the past value of the damper force F into the network input is essential for improving the modeling accuracy. Moreover, results with the input combinations of (x, F) and (x, $\dot{x}$, F) are comparable, while the role played by the displacement x is negligible and it can be excluded to simplify the model architecture. Accordingly, the damper velocity $\dot{x}$ and the past value of damper force F are chosen as the input variables for the NARX network.

After determining the input variables, the selections of the lag spaces ($n_{\dot{x}}$ and n_F) for the input and the number of neurons in the hidden layer (S_2) are addressed. It is assumed that the lag spaces of the velocity and damper force are the same, namely, $n_{\dot{x}} = n_F = L$. Fig. 7 provides the training and validation performance of the NARX network with different input lag spaces. The network is configured with 10 neurons in its hidden layer. The optimal value of the lag space L for each input variable is then chosen to be 4 with the lowest RMS validation error. Once the input variables and the number of input lags are determined, it is simple to decide the number of hidden neurons (S_2) using a trial-and-error procedure by varying the number of hidden neurons from 1 to 25. Fig. 8 shows the modeling performance evaluated on the training and validation data sets as a function of the number of hidden neurons (S_2). It is clear from the figure that the best choice of S_2 is 9 with the minimal value of RMS validation error.

As a result, the NARX network with a topology consisting of 10 input neurons (lag space of 4 for each input variable), 9 hidden neurons and 1 output neuron is configured for modeling the forward dynamics of the self-sensing MR damper.

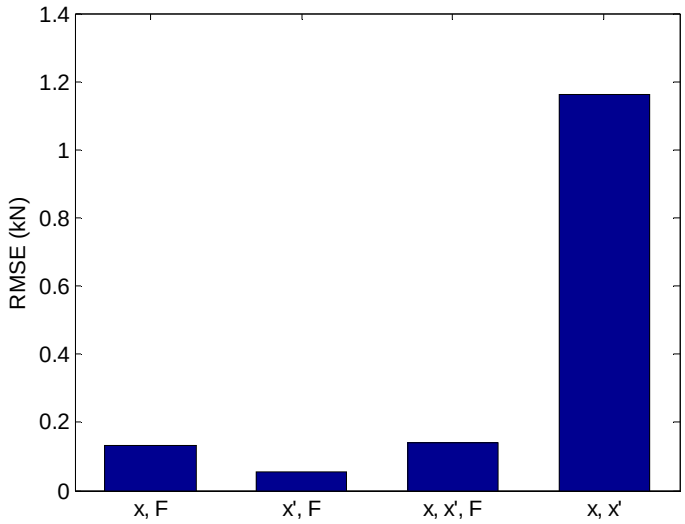

Fig. 6 Performance evaluation over different input configurations

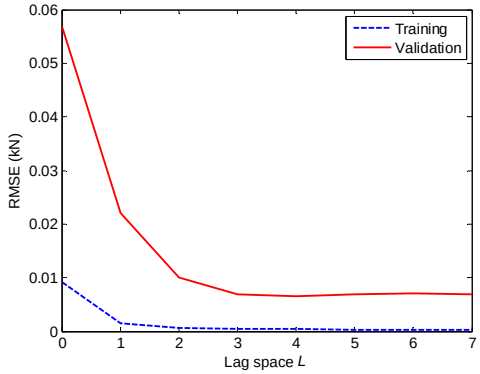

Fig. 7 Performance evaluation over different lag spaces

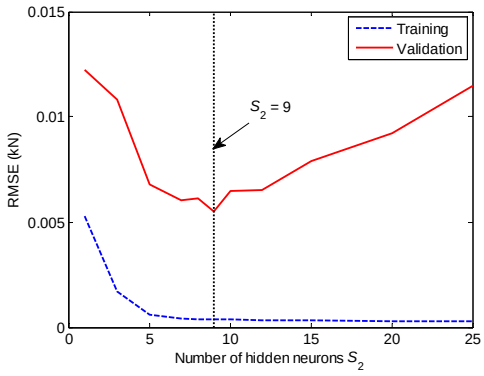

Fig. 8 Performance evaluation over different number of hidden neurons

3.4 Verification

The prediction performance of the well-trained NARX network model is examined using various testing data sets unseen in the training phase. These testing sets are acquired under sinusoidal displacement excitations with frequency of 2.5 Hz and amplitudes of 1.0 mm and 5.0 mm, and under triangular displacement excitations with frequencies of 1.0, 2.5, 5.0 Hz and amplitude of 5.0 mm, as well as with the applied current level held at 0.5 A for the self-sensing MR damper, respectively. They have not been involved in the training phase, and are new for the model assessment. The one-step-ahead damper force is produced from the model once it is exposed to the testing data. Figs. 9-12 plot the hysteresis loops of force-displacement and force-velocity of the damper obtained from the predicted results and the measured data. A comparison between the prediction and the measurement indicates that the NARX network model accurately describes the dynamic behaviors of the self-sensing MR damper, and hence demonstrates its good generalization capability. Likewise, the developed NARX network model can be trained to predict the forward dynamics of the self-sensing MR damper commanded with other input current levels.

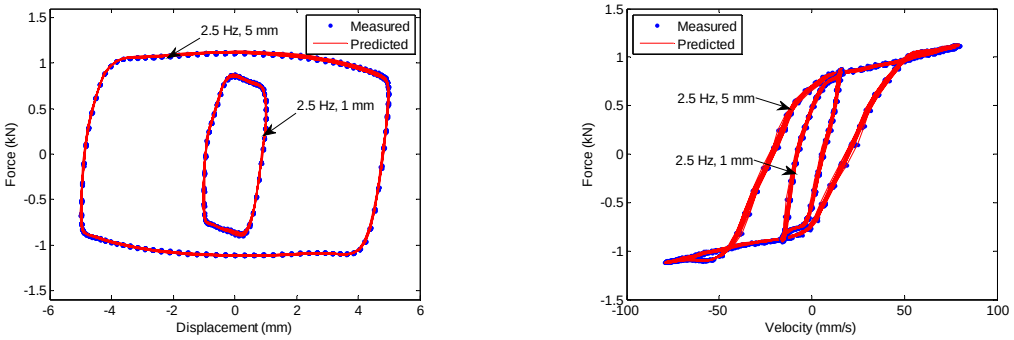

(a) Force versus displacement (b) Force versus velocity

Fig. 9 Generalization result for sinusoidal excitations with frequency of 2.5 Hz and amplitudes of 1.0 mm and 5.0 mm (I = 0.5 A)

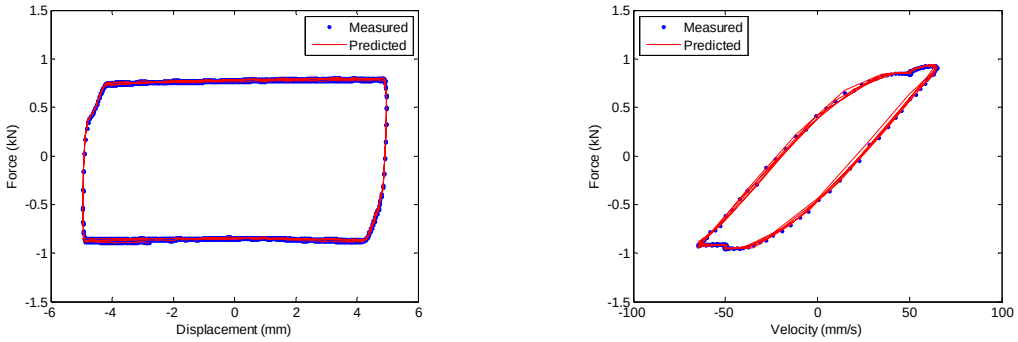

(a) Force versus displacement (b) Force versus velocity

Fig. 10 Generalization result for triangular excitation with frequency of 1.0 Hz and amplitude of 5.0 mm (I = 0.5 A)

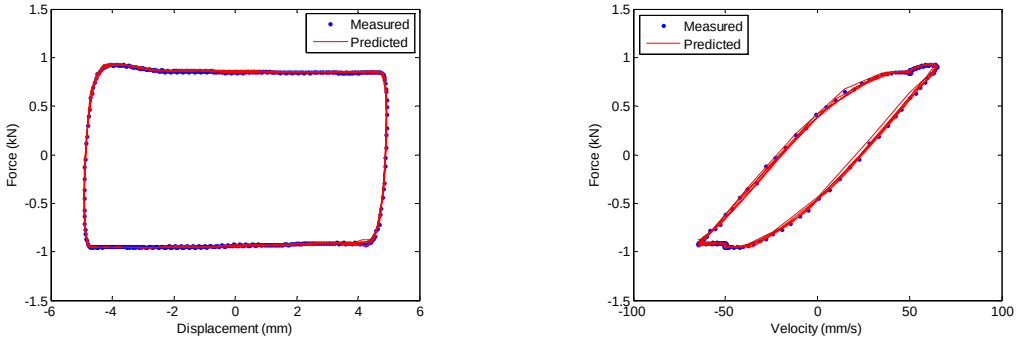

(a) Force versus displacement (b) Force versus velocity

Fig. 11 Generalization result for triangular excitation with frequency of 2.5 Hz and amplitude of 5.0 mm (I = 0.5 A)

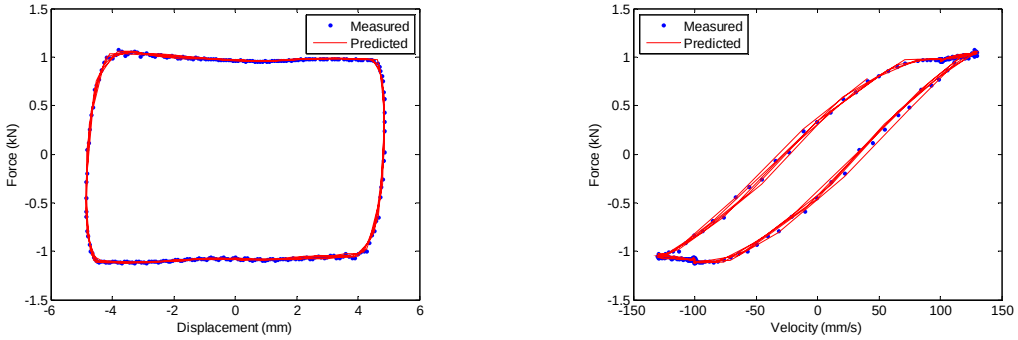

(a) Force versus displacement (b) Force versus velocity

Fig. 12 Generalization result for triangular excitation with frequency of 5.0 Hz and amplitude of 5.0 mm (I = 0.5 A)

4. Extension to time-varying current excitation

The modeling of the self-sensing MR damper presented previously has been based on the cases that the input current applied to the damper was held at a constant level. After recognizing the effectiveness of the previous NARX network model in the current-invariant scenario, it is extended herein to accommodate the situation of time-varying current. Therefore, the formulation in Eq. (5) is extended to include the input quantities of current $I(t)$ and its n_I past values as

$$\hat{F}(t) = f(x(t), \cdots, x(t-n_x), \dot{x}(t), \cdots, \dot{x}(t-n_{\dot{x}}), I(t), \cdots, I(t-n_I), F(t-1), \cdots, F(t-1-n_F); \boldsymbol{\theta}) \quad (11)$$

where $f(\cdot, \boldsymbol{\theta})$ is again an MLP trained by the Levenberg-Marquardt algorithm with Bayesian regularization.

Experimental signals acquired when the self-sensing MR damper is commanded with sinusoidal displacement excitations and random current input are used for the identification of the current-variant model in Eq. (11). The frequency and amplitude of the displacement excitation are 5.0 Hz and 2.5 mm, respectively. The current command is generated using band-limited white noises with amplitude between 0.0 A to 2.0 A and frequency ranging from 0 Hz to 10 Hz. Input and output signals of the damper are recorded at a sampling rate of 500 Hz for 15 s, which produces 7500 samples of data. These data are split into training, validation and testing sets (with a ratio of 4000:2000:1500) for building the NARX network model. Similar to the previously discussed modeling procedure and based on the training and validation data, the input to the NARX network is determined to be the damper velocity ($\dot{x}$), the input current (I) and the past value of the damper force (F) with their lag spaces of $n_{\dot{x}} = n_I = n_F = 4$. The single hidden layer of the NARX network is configured with 20 neurons. Transfer functions in the hidden and output layers are also chosen as a hyperbolic tangent sigmoid function and a linear function, respectively, as given in Eq. (9).

After the model design and optimization steps, the well-trained NARX network is exposed to the testing data for performance evaluation. Fig. 13(a) shows the comparison of the predicted and measured damper forces based on the testing set, and Fig. 13(b) plots the corresponding prediction error. The favorable coincidence between the prediction and the measurement verifies the accurate prediction capacity of the developed forward model for the current-varying case with the RMS

prediction error of 0.038 kN, which is 3.5% of the RMS value of the corresponding target force.

Two more sets of testing data are used to further assess the generalization performance of the formulated model. The testing results are also compared with those obtained from the modified Bouc-Wen phenomenological model proposed by Spencer *et al.* (1997). Testing set 1 is acquired under a sinusoidal displacement excitation with frequency of 1.0 Hz and amplitude of 2.5 mm. Testing set 2 is obtained under a triangular displacement excitation with frequency of 2.5 Hz and amplitude of 2.5 mm. Current inputs for both cases are again generated with band-limited white noises with amplitude between 0.0 to 2.0 A and frequency ranging from 0 to 10 Hz. Figs. 14 and 15 display the predicted forces from the NARX network model and the Bouc-Wen model, which are also compared with the measured ones. The good generalization performance of the NARX network model is demonstrated in Figs. 14(a) and 15(a), in which the prediction matches well with the measurement. Moreover, the NARX network model outperforms the Bouc-Wen model in prediction accuracy, which is also evident from the RMS values of the testing errors summarized in Table 2. It is therefore confirmed that the NARX network model performs with good prediction accuracy and generalization capability, due to its flexibility in modeling and the overfitting control of the Bayesian regularization.

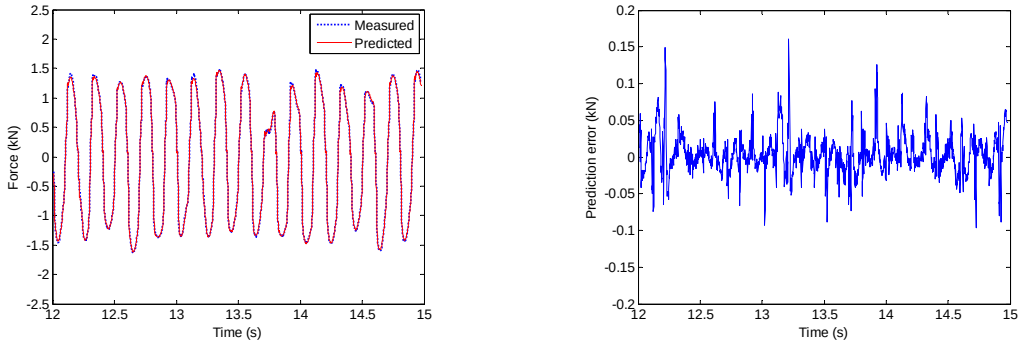

(a) Predicted and measured damper forces (b) Prediction error

Fig. 13 Verification result of NARX network model under time-varying current input

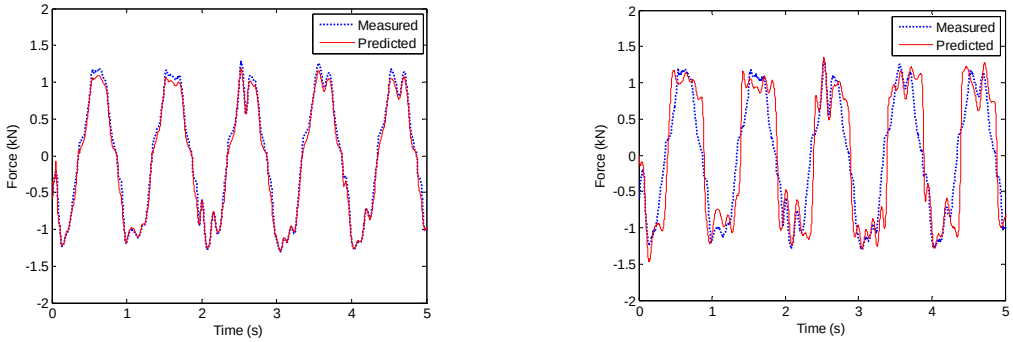

(a) NARX network model (b) Bouc-Wen model

Fig. 14 Comparison of prediction results for testing set 1

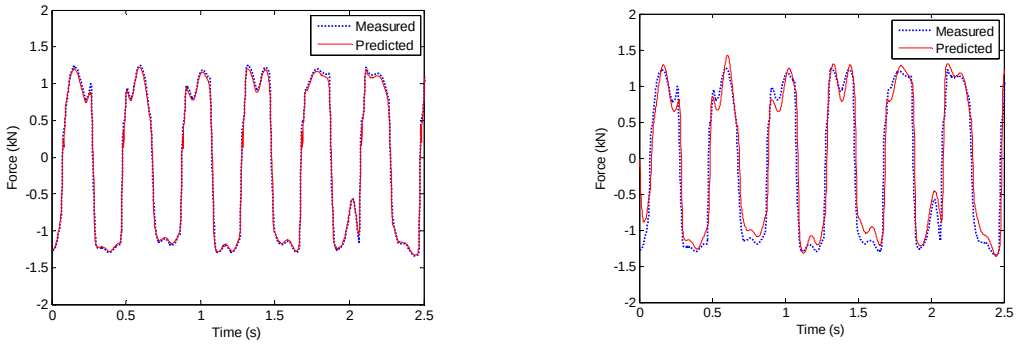

(a) NARX network model (b) Bouc-Wen model

Fig. 15 Comparison of prediction results for testing set 2

Table 2 RMS values of testing errors for damper models

Model	RMSE (kN)	
	Testing set 1	Testing set 2
NARX network	0.078	0.059
Bouc-Wen	0.398	0.269

5. Conclusions

A self-sensing MR damper with embedded piezoelectric force sensor has been devised and characterized to possess an attractive dual-function of sensing-while-damping. The embedded piezoelectric force sensor has shown a high charge-to-force sensitivity under various force-controlled excitations. When subjected to displacement-controlled excitations and commanded with different levels of current input, the self-sensing MR damper has demonstrated excellent force sensing performance as well as controllable damping capability with its inherent highly nonlinear behaviors.

An NARX network model has been developed to emulate the nonlinear forward dynamics of the self-sensing MR damper subjected to harmonic loadings. To enhance its generalization capability, the NARX network was trained by using the Bayesian regularization technique and with optimally configured model architecture. The resulting NARX network model has been verified to accurately describe the nonlinear hysteretic behaviors of the self-sensing MR damper in the constant current settings when exposed to novel testing data. With the success, the NARX network model has been further extended to accommodate the scenario of time-varying current. Testing results have verified that the current-variant NARX network model significantly outperforms a Bouc-Wen based parametric model in both prediction accuracy and generalization capability, due to its flexibility and the overfitting control by the Bayesian regularization.

It is worth mentioning that all the experimental data used for the NARX network modeling in this study were obtained from the self-sensing MR damper subjected to harmonic loading. To ensure generalization and robustness of the damper model in practical control circumstances, further investigation is in need to be conducted by presenting the developed NARX network model to random loading conditions.

Acknowledgments

The work described in this paper was supported in part by a grant from The Hong Kong Polytechnic University (Project No. 4-BC01) and partially by a grant from the Innovation and Technology Support Programme of the Hong Kong Special Administrative Region, China (Project No. ITS/241/11).

References

Ahn, K.K., Truong, D.Q. and Islam, M.A. (2009), "Modeling of a magneto-rheological (MR) fluid damper using a self tuning fuzzy mechanism", *J. Mech. Sci. Technol.*, **23**(5), 1485-1499.

Boada, M.J.L., Calvo, J.A., Boada, B.L. and Díaz, V. (2011), "Modeling of a magnetorheological damper by recursive lazy learning", *Int. J. Nonlinear Mech.*, **46**(3), 479-485.

Boston, C., Weber, F. and Guzzella, L. (2010), "Modeling of a disc-type magnetorheological damper", *Smart Mater. Struct.*, **19**(4), 045005.

Cao, M., Wang, K.W. and Lee, K.Y. (2008), "Scalable and invertible PMNN model for magneto-rheological fluid dampers", *J. Vib. Control*, **14**(5), 731-751.

Carlson, J.D., Catanzarite, D.M. and Clair, K.A.St. (1996), "Commercial magneto-rheological fluid devices", *Int. J. Modern Phys. B*, **10**(23-24), 2857-2865.

Chang, C.C. and Roschke, P.N. (1998), "Neural network modeling of a magnetorheological damper", *J. Intel. Mater. Syst. Struct.*, **9**(9), 755-764.

Chen, S., Billings, S.A., Cowan, C.F. and Grant, P.M. (1990), "Practical identification of NARMAX models using radial basis functions", *Int. J. Control*, **52**(6), 1327-1350.

Chen, Z.Q., Wang, X.Y., Ko, J.M., Ni, Y.Q., Spencer, B.F., Yang, G. and Hu, J.H. (2004), "MR damping system for mitigating wind-rain induced vibration on Dongting Lake Cable-Stayed Bridge", *Wind Struct.*, **7**(5), 293-304.

Choi, S.B., Seong, M.S. and Ha, S.H. (2009), "Vibration control of an MR vehicle suspension system considering both hysteretic behavior and parameter variation", *Smart Mater. Struct.*, **18**(12), 125010.

Duan, Y.F., Ni, Y.Q. and Ko, J.M. (2005), "State-derivative feedback control of cable vibration using semiactive magnetorheological dampers", *Comput. - Aided Civil Infrastruct. Eng.*, **20**(6), 431-449.

Dyke, S.J., Spencer, B.F. Jr., Sain, M.K. and Carlson, J.D. (1996), "Modeling and control of magnetorheological dampers for seismic response reduction", *Smart Mater. Struct.*, **5**(5), 565-575.

Foresee, F.D. and Hagan, M.T. (1997), "Gauss-Newton approximation to Bayesian learning", *Proceedings of the 1997 IEEE International Joint Conference on Neural Networks*, Houston, USA, June.

Fujitani, H., Sodeyama, H., Tomura, T., Hiwatashi, T., Shiozaki, Y., Hata, K., Sunakoda, K., Morishita, S. and Soda, S. (2003), "Development of 400kN magnetorheological damper for a real base-isolated building", *Proceedings of the SPIE*, *Smart Structures and Materials 2003: Damping and Isolation*, (Eds., G.S. Agnes and K.W. Wang), San Diego, CA, USA, March.

Gandhi, F., Wang, K.W. and Xia, L. (2001), "Magnetorheological fluid damper feedback linearization control for helicopter rotor application", *Smart Mater. Struct.*, **10**(1), 96-103.

Gordaninejad, F., Saiidi, M., Hansen, B.C., Ericksen, E.O. and Chang, F.-K. (2002), "Magneto-rheological fluid dampers for control of bridges", *J. Intel. Mat. Syst. Str.*, **13**(2-3), 167-180.

Hagan, M.T. and Menhaj, M.B. (1994), "Training feedforward networks with the Marquardt algorithm", *IEEE T. Neural Networ.*, **5**(6), 989-993.

Hornik, K., Stinchcombe, M. and White, H. (1989), "Multilayer feedforward networks are universal approximators", *Neural Networks*, **2**(5), 359-366.

Hu, W. and Wereley, N.M. (2008), "Hybrid magnetorheological fluid-elastomeric lag dampers for helicopter stability augmentation", *Smart Mater. Struct.*, **17**(4), 045021.

Ikhouane, F. and Dyke, S.J. (2007), "Modeling and identification of a shear mode magnetorheological damper", *Smart Mater. Struct.*, **16**(3), 605-616.
Jiménez, R. and Álvarez-Icaza, L. (2005), "LuGre friction model for a magnetorheological damper", *Struct. Control Health Monit.*, **12**(1), 91-116.
Jin, G., Sain, M.K. and Spencer, B.F. Jr. (2005), "Nonlinear blackbox modeling of MR-dampers for civil structural control", *IEEE T. Contr. Sys. T.*, **13**(3), 345-355.
Johnson, E.A., Baker, G.A., Spencer, B.F. Jr. and Fujino, Y. (2000), "Mitigating stay cable oscillation using semiactive damping", *Proceedings of the SPIE, Smart Structures and Materials 2000: Smart Systems for Bridges, Structures, and Highways*, S.-C. Liu (ed.), Newport Beach, USA, March.
Jung, H.J., Spencer, B.F. Jr. and Lee, I.W. (2003), "Control of seismically excited cable-stayed bridge employing magnetorheological fluid dampers", *J. Struct. Eng. - ASCE*, **129**(7), 873-883.
Jung, H.J., Spencer, B.F. Jr., Ni, Y.Q. and Lee, I.W. (2004), "State-of-the-art of semiactive control systems using MR fluid dampers in civil engineering applications", *Struct. Eng. Mech.*, **17**(3), 493-526.
Karimi, H.R., Zapateiro, M. and Luo, N. (2009), "Wavelet-based parameter identification of a nonlinear magnetorheological damper", *Int. J. Wavelets Multi.*, **7**(2), 183-198.
Ko, J.M., Ni, Y.Q., Chen, Z.Q. and Spencer, B.F. Jr. (2002), "Implementation of magneto-rheological dampers to Dongting Lake Bridge for cable vibration mitigation", *Proceedings of the 3rd World Conference on Structural Control*, F. Casciati (ed.), Como, Italy, April.
Leva, A. and Piroddi, L. (2002), "NARX-based technique for the modelling of magneto-rheological damping devices", *Smart Mater. Struct.*, **11**(1), 79-88.
Li, H., Liu, M., Li, J., Guan, X. and Ou, J. (2007), "Vibration control of stay cables of the Shandong Binzhou Yellow River Highway Bridge using magnetorheological fluid dampers", *J. Bridge Eng.*, **12**(4), 401-409.
Liao, W.H. and Wang, D.H. (2003), "Semiactive vibration control of train suspension systems via magnetorheological dampers", *J. Intel. Mat. Syst. Str.*, **14**(3), 161-172.
Loh, C.H., Lynch, J.P., Lu, K.C. and Wang, Y. (2007), "Experimental verification of a wireless sensing and control system for structural control using MR dampers", *Earthq. Eng. Struct. D.*, **36**(10), 1303-1328.
MacKay, D.J.C. (1992), "A practical Bayesian framework for backprop networks", *Neural Comput.*, **4**(3), 448-472.
Ni, Y.Q., Ying, Z.G., Wang, J.Y., Ko, J.M. and Spencer, B.F. Jr. (2004), "Stochastic optimal control of wind-excited tall buildings using semi-active MR-TLCDs", *Probabilist. Eng. Mech.*, **19**(3), 269-277.
Or, S.W., Duan, Y.F., Ni, Y.Q., Chen, Z.H. and Lam, K.H. (2008), "Development of magnetorheological dampers with embedded piezoelectric sensors for structural vibration control", *J. Intel. Mat. Syst. Str.*, **19**(11), 1327-1338.
Pang, L., Kamath, G.M. and Wereley, N.M. (1998), "Analysis and testing of a linear stroke magnetorheological damper", *Proceedings of the AIAA/ASME/AHS Adaptive Structures Forum*, Long Beach, CA, April.
Schurter, K.C. and Roschke, P.N. (2000), "Fuzzy modeling of a magnetorheological damper using ANFIS", *Proceedings of the 9th IEEE International Conference on Fuzzy Systems*, San Antonio, USA, May.
Sjöberg, J. and Ljung, L. (1995), "Overtraining, regularization and searching for minimum, with application to neural networks", *Int. J. Control*, **62**(6), 1391-1407.
Song, X., Ahmadian, M., Southward, S. and Miller, L.R. (2005), "An adaptive semiactive control algorithm for magnetorheological suspension systems", *J. Vib. Acoust.*, **127**(5), 493-502.
Spencer, B.F. Jr., Dyke, S.J., Sain, M.K. and Carlson, J.D. (1997), "Phenomenological model for magnetorheological dampers", *J. Eng. Mech.- ASCE*, **123**(3), 230-238.
Suykens, J.A.K., Vandewalle, J.P.L. and De Moor, B.L.R. (1996), *Artificial Neural Networks for Modeling and Control of Non-linear Systems*, Kluwer Academic Publishers, Boston, USA.
Wang, D.H. and Liao, W.H. (2005), "Modeling and control of magnetorheological fluid dampers using neural networks", *Smart Mater. Struct.*, **14**(1), 111-126.
Weber, F., Distl, H., Feltrin, G. and Motavalli, M. (2005a), "Evaluation procedure of decay measurements of a cable with passive-on operating MR damper", *Proceedings of the 6th International Symposium on Cable*

Dynamics, Charleston, USA, September.
Weber, F., Distl, H., Feltrin, G. and Motavalli, M. (2005b), "Simplified approach of velocity feedback for MR dampers on real cable-stayed bridges", *Proceedings of the 6th International Symposium on Cable Dynamics*, Charleston, USA, September.
Ying, Z.G., Ni, Y.Q. and Ko, J.M. (2005), "Semi-active optimal control of linearized systems with multi-degree of freedom and application", *J. Sound Vib.*, **279**(1-2), 373-388.

CY